A look inside of diamond-forming media in deep subduction zones

Larissa F. Dobrzhinetskaya, Richard Wirth, and Harry W. Green, II

PNAS published online Mar 26, 2007;
doi:10.1073/pnas.0609161104

A look inside of diamond-forming media in deep subduction zones

Larissa F. Dobrzhinetskaya*†, Richard Wirth‡, and Harry W. Green II*

*Department of Earth Sciences and Institute of Geophysics and Planetary Physics, University of California, Riverside, CA 92521; and ‡GeoForschungsZentrum, D-14473, Potsdam, Germany

Edited by Ho-kwang Mao, Carnegie Institution of Washington, Washington, DC, and approved February 22, 2007 (received for review October 17, 2006)

Geologists have ''known'' for many years that continental crust is buoyant and cannot be subducted very deep. Microdiamonds 10–80 μm in size discovered in the 1980s within metamorphic rocks related to continental collisions clearly refute this statement, suggesting that material of continental crust has been subducted to a minimum depth of >150 km and incorporated into mountain chains during tectonic exhumation. Over the past decade, the rapidly moving technological advancement has made it possible to examine these diamonds in detail, and to learn that they contain nanometric multiphase inclusions of crystalline and fluid phases and are characterized by a ''crustal'' signature of carbon stable isotopes. Scanning and transmission electron microscopy, focused ion beam techniques, synchrotron infrared spectroscopy, and nano-secondary ion mass spectrometry studies of these diamonds provide evidence that they were crystallized from a supercritical carbon-oxygen-hydrogen fluid. These microdiamonds preserve evidence of the pathway by which carbon and water can be subducted to mantle depths and returned back to the earth's surface.

crust | microdiamonds | fluid

Diamond, built by densely packed carbon atoms, is valued as a gemstone and as a unique industrial/technological material because of its extraordinary hardness, transparency, and high thermal conductivity, and could become a semiconductor when doped with boron or other components (1, 2). With the exception of impact microdiamonds, all natural diamonds are formed in the earth's deep interior (upper mantle, mantle transition zone, and some of them even below the 660-km seismic discontinuity). They are delivered to the earth's surface by volatile-rich kimberlite or related magmas rising up through pipe-like structures together with abundant fragments of wall rocks from the base of the lithosphere. Because of its chemical inertness, diamond is a near-perfect container, stable for long geological times, for fluid and solid inclusions that are trapped during its growth. The chemistry and structure of inclusions are used to reconstruct mantle mineralogy, and conditions and compositions of diamond-forming media.

A new, nonvolcanic type of diamond-bearing rocks was discovered >25 years ago but not made known to the western literature until 1990. These are metasedimentary rocks in orogenic belts formed at convergent plate boundaries in Paleozoic–Mesozoic (≈480–250 Ma) time. Five well confirmed diamond-bearing terranes, the Kokchetav massif of Kazakhstan (3), Dabie and Quinlin in China (4, 5), the Western Gneiss Region of Norway (6, 7), the Erzgebirge massif of Germany (8), and the Kimi complex of the Greek Rhodope (9), are established now. In these localities the diamonds are characterized by small (1–80 μm) crystals of skeletal, cuboidal, subrounded, and other imperfect morphologies (10, 11). The nitrogen impurities in diamonds from Kazakhstan, Norway, and Germany suggest that all of them belong to the type 1b-1aA, implying a short residence time at high temperature (≈900–1,100°C) of ≈5 Ma (6, 12, 13), which distinguishes them from other nitrogen-bearing diamonds of kimberlitic sources (type 1aAB), having much longer residence time in the earth's interior (12, 14). The presence of microdiamonds within rocks of continental affinity suggests that these rocks, despite their intrinsic buoyancy, were subducted into the upper mantle to a minimum depth of 150 km and subsequently exhumed to the earth's surface. This discovery spurred unprecedented multidisciplinary investigations of continental collisions, mountain building, mantle enrichment in H_2O, and rare earth and lithophile elements, including ^{40}K, which has strong influence on the earth's thermal evolution. The discovery of these microdiamonds, as well as coesite, triggered a major revision in understanding of deep subduction processes, leading to the realization that continental materials can be recycled into the earth's interior, and establishing a new scientific discipline, ultra-high-pressure metamorphism.

The last 5 years were also marked by technological progress in development of new instrumentations and techniques. A series of high-resolution analytical instruments, which primarily were built for condensed matter physics and materials science, have recently become available for the study of earth's materials, allowing us to recognize nanometric solid and fluid inclusions incorporated in microdiamonds and establish their chemical composition and structure. This new direction, nanoscale geoscience, had a major impact on establishing a sound correlation between results obtained with different techniques such as synchrotron light sources, focused ion beam (FIB)-assisted high-resolution transmission and scanning electron microscopy (TEM and SEM), and nano-secondary ion mass spectrometry (nanoSIMS) applied to natural microdiamonds and their synthetic analogues. We have used these instruments to study microdiamonds from Erzgebirge, Germany. The integrated results provide valuable information that strongly supports the concept of diamond crystallization from a carbon-oxygen-hydrogen (COH) supercritical fluid and emphasizes the role of a ''crustal'' source of carbon.

Diamond Morphology

A high concentration of microdiamonds occurs in quartzofeldspathic gneisses from the Late Paleozoic crystalline massif of Erzgebirge, Germany (8, 15). These rocks were collected from small outcrops in the vicinity of the Saidenbach water reservoir, ≈1.5 km northwest of the village of Forchheim in the Saxonian Erzgebirge. In addition to quartz and feldspar, the rocks contain garnet and phengite and other accessory minerals; the rocks were subjected to ultra-high-pressure metamorphism at ≈1,100°C and P = 7–8 GPa (15). Most Erzgebirge diamonds occur as inclusions in garnet and zircon; some are situated at the grain boundaries of phengite, quartz, and garnet, suggesting that

Author contributions: L.F.D. designed research; L.F.D. and R.W. performed research; L.F.D. and R.W. contributed new reagents/analytic tools; L.F.D. and H.W.G. analyzed data; and L.F.D. and H.W.G. wrote the paper.

The authors declare no conflict of interest.

This article is a PNAS Direct Submission.

Abbreviations: FIB, focused ion beam; nanoSIMS, nano-secondary ion mass spectrometry; STEM, scanning transmission electron microscopy; TEM, transmission electron microscopy.

†To whom correspondence should be addressed. E-mail: larissa@ucr.edu.

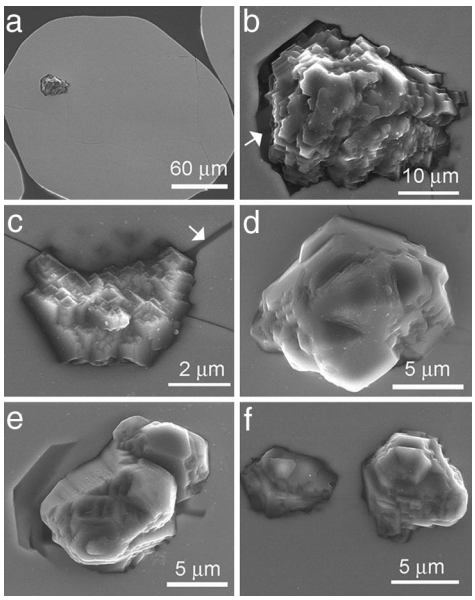

Fig. 1. Secondary electron images (SEM) of the microdiamonds from the Erzgebirge massif, Germany, included in zircon. (*a*) An entire grain of zircon containing a single diamond inclusion. (*b*) A magnified image of this diamond shows phengite (arrowhead) situated at the diamond-zircon boundary. (*c*) The top of another diamond crystal exposed on the flat surface of zircon: the rough surface of diamond consists of myriad small facets of variable size representing almost all orientations of {111} complicated by rare small triangular etch pits. The arrow indicates phengite. (*d*) A diamond crystal with dominating octahedral faces truncated at the corners and along their edges, and triangle pits of various scale. (*e*) Two adjacent diamond crystals characterized by combinations of cuboidal and octahedral faces and small triangular etch pits. At the left side of the diamond there is a depression that was filled by phengite that was partly removed during polishing. (*f*) Two small irregular islands of diamond whose facets suggest that they may be two lobes of a single crystal.

they might have crystallized from a fluid (16, 17). These diamonds exhibit diverse morphologies as seen in polished rockslides and in zircon separates using SEM secondary electron imaging (Fig. 1). Because of slight chemical etching by our colloidal silica polishing system (10, 18), the diamonds stand out above the flat surface of host zircons, allowing the observation of details of crystal shapes. A single diamond crystal shown in Fig. 1*b* is surrounded by phengite and has a complicated shape characterized by a combination of low crystallographic index "microplates," most probably {111} [110]. The top of another crystal (Fig. 1*c*) consists of myriad small facets representing almost all orientations of {111} complicated by rare small triangular pits. The shape of many other Erzgebirge diamonds is characterized by a combination of cuboidal and octahedral faces complicated with sharp truncated corners and presence of hillocks and triangle pits of various scale (Fig. 1 *d–f*). Such diamond morphologies suggest that they were formed in a medium oversaturated with impurities, and that the rate of deposition of carbon atoms at the corners and on the faces of diamond nuclei was different, providing faster growth of the crystal edges (10, 19).

Nanometric Solid and Fluid Inclusions in Diamonds

The nanometric inclusions in diamonds are pristine witnesses of the medium from which diamond was crystallized. Direct TEM examination of fluid inclusions was not possible (20) until recently when the FIB technique became available for high-quality foil preparation (10, 16, 21, 22). Our first results of FIB/TEM studies of Erzgebirge diamonds (16) revealed that they contain dozens of nanometric crystalline inclusions. Some inclusions are chemically simple and may be classified as SiO_2 and Al_2SiO_5 according to their stoichiometry, but most contain Ti, P, K, Si, Fe, and O in nonstoichiometric combinations and proportions (16). Some are amorphous, whereas others are crystalline. Many nanometric cavities surrounded by thin amorphous films containing Ca, K, Si, and Fe occur and were interpreted as traces of evaporated fluid, bubbles of which were penetrated by Ga^+ beam during FIB foil preparation. However, similar amorphous matter in Erzgebirge diamonds was interpreted by Hwang *et al.* (23) as evidence of silicate melt, which was proposed as a medium of diamond crystallization.

We have now resolved this controversy by applying two independent advanced techniques to study both solid and fluid nanoscale inclusions in microdiamonds. A single diamond crystal (diamond #1) extracted from sample 0015 was subjected first to synchrotron IR spectroscopy (Fig. 2) and later to TEM examination assisted by the FIB foil preparation technique (Fig. 3). Results of synchrotron IR spectra of this and other diamonds (24) indicate absorptions corresponding to stretching and bending motions of the H_2O molecule and carbonate radical $(CO_3)^{2-}$. Nitrogen-related absorptions with a strong peak at 1,282 cm^{-1} and small but well pronounced peaks at 1,130 cm^{-1} and 1,134 cm^{-1} confirm that these diamonds belong to type 1b-1aA, similar to Kokchetav diamonds (12). The IR spectrum of diamond #1 (Fig. 2*b*) suggests that this diamond contains fluid inclusions and/or probably water-bearing crystalline and carbonate phases.

Several multiphase nanoinclusions were found in a standard FIB foil (#1042) of diamond #1 prepared according to proce-

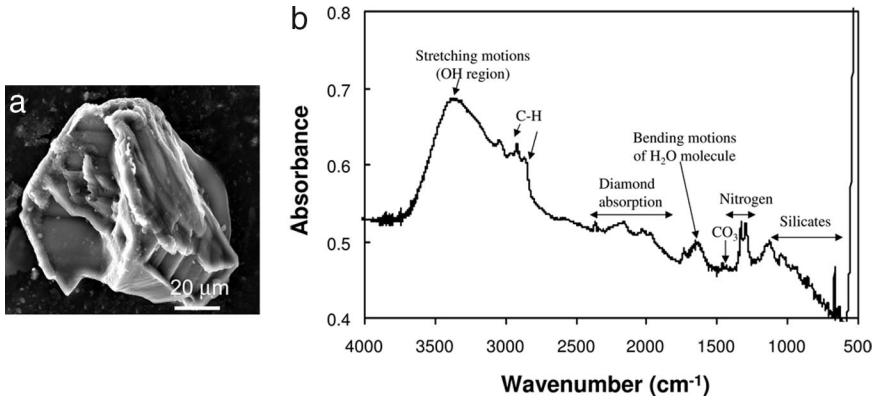

Fig. 2. Synchrotron IR spectrometry data. (*a*) Secondary electron image (SEM) of diamond #1 from the Erzgebirge gneiss selected for both synchrotron IR research and for FIB-assisted TEM studies (Fig. 3). (*b*) Synchrotron IR spectrum of diamond #1. [Reproduced with permission from ref. 24 (Copyright 2006, Elsevier).]

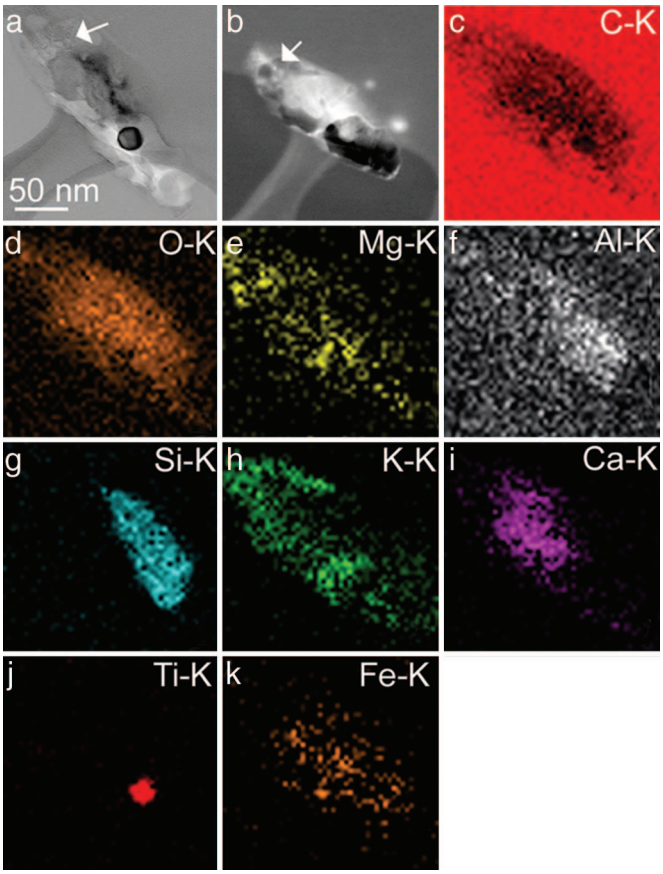

Fig. 3. Elemental mapping of multiphase (fluid plus solid) inclusion. (*a*) Bright-field high-resolution TEM image of multiphase inclusion A taken early in analysis; fluid phase movement caused by beam heating was observed in the upper left (arrow) and lower right parts of this composite inclusion. (*b*) STEM image of the same inclusion taken late in analysis after the lower right corner of the inclusion burst (black). (*c–k*) Individual maps of the K-lines of the following elements: O, Mg, Al, Si, K, Ca, Ti, and Fe. See the text for further explanation.

dures described earlier (16, 22). The largest inclusion A (350 × 80 nm) is described here in detail. A diffraction contrast image (Fig. 3*a*) indicates that the inclusion consists of both crystalline and fluid phases. The latter was confirmed by the "movement" of the upper-left portion of the inclusion due to electron beam heating.

Elemental mapping of inclusion A was performed to determine the spatial distribution of chemical components. Fig. 3 *c–k* shows elemental maps of the K-lines of C, O, Mg, Al, Si, K, Ca, Ti, and Fe, respectively. The high Ti area in Fig. 3*i* lies within a very bright area in the O image (Fig. 3*d*), suggesting that the round black crystal of Fig. 3*a* is TiO_2, with minor Fe content (Fig. 3*k*). The crystal structure of the TiO_2 nanocrystal cannot be resolved, but it could be TiO_2 with α-PbO_2 structure, because this phase is syngenetic to diamond and has been reported previously from these rocks (25). The high Si region is very tightly defined (Fig. 3*g*); in addition to overlapping with the Ti concentration, it correlates well with Al and O, indicating the probable presence of an aluminosilicate, probably kyanite, or phase "Egg" [$AlSiO_3(OH)$], or topaz-OH [$Al_2SiO_4(OH)_2$]. The Mg distribution (Fig. 3*e*) shows two separate concentrations. Using the FEI software, which supports the EDAX system, we can correlate "pixel by pixel" the Mg content with other elements. The computer simulation shows that Mg correlates with Al, Si, Fe, and especially K, thereby suggesting that the high K

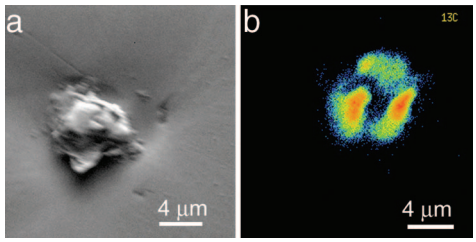

Fig. 4. Carbon isotopic heterogeneity. (*a*) Secondary electron image of single diamond included in garnet from the Erzgebirge massif, Germany. (*b*) ^{13}C map of the diamond by nanoSIMS CAMECA 50.

area (Fig. 3*h*) near the TiO_2 crystal may represent a mica (phengite or phlogopite?), whereas the high K-Mg regions in the upper left suggest residue from fluid contents. The high Ca region contains high O and low Fe, K, and Mg but no Si and Al and Ti. Because the high Ca area was one of those that have exhibited a "pulse-like" movement caused by electron beam heating, we assume that this area is at least partially fluid, which could explain the weak correlations. A fluid of similar composition was previously described from a Kokchetav microdiamond (26, 27), and it is associated with aragonite crystals. However, the Ca signal of this Erzgebirge fluid phase does not correlate positively with C (Fig. 3*c*). Thus, the high Ca region may represent a carbonate with small admixture of Fe and Mg; it also could represent CaO, CaF_2, or $Ca(OH)_2$, none of which have been previously identified in diamonds. On the other hand, the presence of carbonate absorptions in the IR spectra summarized above strongly suggests that carbonates are present within this diamond.

The interpretation of elemental mapping of multiphase inclusion A in diamond shows that these two independent analytical techniques, synchrotron IR spectrometry and FIB-assisted scanning transmission electron microscopy (STEM), reveal coherent and complementary information related to composition of the nanoinclusions. From synchrotron IR spectra, the stretching motion of H_2O indicates the presence of OH radical, which is supported by the presence of mica (phengite or phlogopite?) nanoinclusions established by the STEM elemental mapping, and the H_2O bending absorptions identify H_2O as a component of the fluid. The lower right part of multiple inclusion A burst during beam heating near the end of the STEM session (compare the mottled contrast in Fig. 3*a* with the dark contrast in Fig. 3*b*).

Overall, our data obtained by these techniques suggest that the Erzgebirge microdiamonds grew from a supercritical carbon-oxygen-hydrogen (COH) fluid during the course of ultra-high-pressure metamorphism (16, 17), as has been argued previously for Kokchetav microdiamonds (10, 11, 16).

Origin of Carbon from Which Diamonds Were Crystallized

A $\delta^{13}C$ value and the nitrogen content are widely used to constrain conditions of formation and the source of media (fluid/melt) from which diamonds are crystallized (12, 14). The Kokchetav diamonds from garnet-pyroxenite rocks contain $\delta^{13}C = -10.57‰$ and $N = 11{,}150$ ppm, whereas diamonds from dolomitic marble are characterized by $\delta^{13}C = -10.19‰$ and $N = 2{,}650$ ppm; these $\delta^{13}C$ values have been interpreted as a mixture of mantle and crustal carbon reservoirs (10, 12). Our carbon isotope studies performed on the Erzgebirge microdiamonds (Fig. 4) show that they are characterized by unusually "light" carbon isotope signatures in comparison with that of the Kokchetav massif. Seven studied diamond crystals hosted by garnets of the Erzgebirge gneisses are characterized by $\delta^{13}C =$

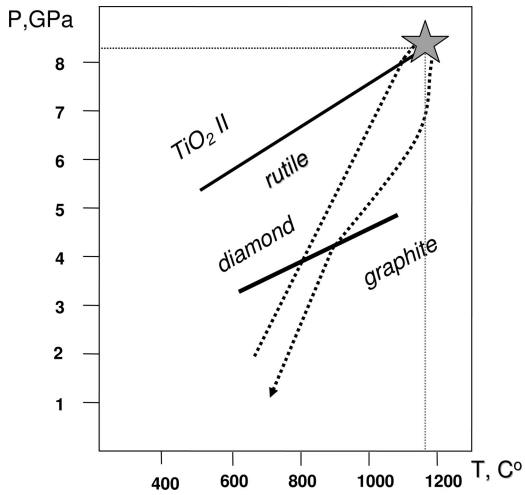

Fig. 5. Pressure vs. temperature phase diagram, with exhumation curve. The heavy black straight lines show boundaries separating the stability fields of rutile and TiO_2 II (with αPbO_2 structure), and of graphite and diamond. The dotted curve shows the P-T path of the Erzgebirge diamond-bearing quartzofeldspathic rocks containing TiO_2 II. The star indicates the minimum peak of P and T conditions reached by the Erzgebirge metasedimentary rocks during their subduction. [Reproduced with permission from ref. 15 (Copyright 2003, Elsevier).]

$-17‰$ to $-27‰$ and $N = 100–4{,}647$ ppm.[§] The ranges of $\delta^{13}C$ suggest that Erzgebirge diamonds were crystallized from "crustal" carbon, either of organic or inorganic origin. The wide ranges of nitrogen may be attributed to an inhomogeneous distribution of inclusions of nitrogen-bearing fluid, or N-bearing mica within microdiamonds. It could also result from the different rate of nitrogen incorporation into diamond structure during its crystallization.

Depth of Diamond Crystallization and Rate of Exhumation

The minimum subduction depth of Erzgebirge diamond-bearing gneisses has been suggested to be 7–8 GPa, based on the presence of TiO_2 with the α-PbO_2 structure (15, 25, 29) (Fig. 5). The nitrogen impurities in Erzgebirge diamonds include single N defects and N pairs (23), resulting in their classification as type 1b-1aA; the detection of a 1b component (single N atoms) suggests the possibility for very fast exhumation (<1 million years) (12, 30, 31). Because of the rather low activation energy ($\approx$4.4 eV) for single N atoms to aggregate into N pairs, the occurrence of nitrogen impurities as single atoms in the crystal lattice implies that the Erzgebirge diamonds had a short residence time: indeed, at a temperature of 700°C, any diamond with N content of >100 ppm would be type 1aA within 1 million years (12, 30, 31). Because currently our data on nitrogen contents are too limited for quantitative calculation of the rate of exhumation of the Erzgebirge diamond-bearing rocks, we refer to numerical modeling according to which exhumation from ultra-high-pressure metamorphism conditions occurred during 1–5 million years (13).

Summary and Perspectives

The wide range of data on the Erzgebirge microdiamonds, including their imperfect morphology, diverse composition of multiphase nanoscale inclusions, character of nitrogen aggregation, and "crustal" carbon reservoir signature, are consistent with the concept of diamond crystallization from a supercritical COH fluid during the ultra-high-pressure metamorphism related to continental collision. This may be the first example where synergy of advanced scientific technology and instrumentation applied to microdiamonds collected from the same locality have produced complementary data allowing the construction of a coherent picture of subduction-zone diamond formation. These observations are consistent with diamonds synthesized at high pressure and high temperature from graphite, amorphous carbon, and coal in the presence of H_2O (32–35).

One more message from our high-resolution investigation of microdiamonds is the establishment of their $\delta^{13}C$ signatures. This, together with multiphase fluid–solid nanometric inclusions, provides evidence for a pathway by which light "crustal" carbon could be subducted to the mantle depths and back to the earth's surface. Such observations of nanoscale geological features have become possible only recently because of rapid progress of scientific technology and analytical instrumentation, thus providing new interpretations of microdiamond origins and advanced study of plate tectonics, mantle geochemistry, and the carbon cycle.

Synergy of Different Methods and Analytical Techniques

Sample Preparation. Polished thick rock slides or zircon single grains mounted by petropoxy on a standard petrographic glass slide were prepared from the specimens by conventional polishing techniques using SiC and Al_2O_3 grids of 100, 14, and 3 μm size. With a final polishing using the SiO_2 colloidal system of 0.06 μm, we were able to polish host zircons and garnets to let the denser diamond inclusions stand out above the zircon/garnet surface (6, 16, 18). Diamond crystals were also separated from the rocks by a microwave method of thermochemical digesting (24) to evaluate details of their morphologies and to use single crystals for further synchrotron radiation research.

Scanning Electron Microscopy. SEM was used to characterize microdiamond morphologies and to establish diamond association with other surrounding minerals. SEM was performed at the University of California at Riverside with a Philips XL30 instrument equipped with a field emission gun and EDAX microanalytical system operating at 15 and 20 kV. The latter consists of an energy-dispersive x-ray spectrometer equipped with a Si detector with a superultrathin window and a resolution of 137 eV MnK_α. The spectral data were acquired at 1,500–2,000 counts per second with dead time below 25%, a beam current of $\approx$1 nA, and an effective spot size of $\approx$1.5 μm. The diamond images were acquired at secondary electron mode with a spot size of 3 and a working distance of 10 units.

Synchrotron IR Microspectroscopy. Synchrotron radiation, a very bright source of IR photons, consists of low-energy (0.05–0.5 eV) mid-IR photons, which neither break the chemical bonds nor cause ionization or heating of the sample. The intense synchrotron source provides IR spectra with high signal-to-noise ratios at spatial resolutions as fine as 3–10 μm. To measure light elements, such as H, O, and N, and their bonding or aggregation with/around C atoms of microdiamonds, we used beamline U2A of the National Synchrotron Light Source at the Brookhaven National Laboratory (Upton, NY). The optical layout of the beamline facility is described in detail in ref. 36. The diamond IR spectra were collected with a Bruker IFS 66v/S vacuum Fourier transform interferometer interfaced with the synchrotron source and a modified Bruker IRscope II microscope equipped with an HgCdTe type-A detector. The top aperture/field stop was set to 10×10 μm^2, and the spectra were acquired in the range of 600–4,000 cm^{-1} with a KBr beam splitter. The optical bench was evacuated, and the microscope was purged with dry nitrogen gas during the measurements to reduce or eliminate water vapor absorption.

[§]Takahata, N., Sano, Y., Shirai, K., Dobrzhinetskaya, L. F., Green, H. W., *Fall AGU Meeting*, Dec. 5–9, 2005, San Francisco, CA, abstr. F-1234.

FIB-Assisted TEM. FIB-assisted TEM was performed to study nanometric inclusions incorporated in microdiamonds to understand the media of diamond crystallization. The FIB is a novel technique that primarily was developed in the late 1980s (37) to facilitate the assembly of computer microdevices, diagnosis of their failure, and their repair. Later, this technique was applied to the examination of silicon wafers in the semiconductor industry, fabrication of nanotube devices, and many other needs of the modern high-tech industry (38). During the last 4–5 years, FIB has become an important instrument for the preparation of hundred-angstrom-thick foils from terrestrial and extraterrestrial geological materials for their further study by TEM (17, 21, 22). In earth sciences, the FIB system is used for *in situ* sectioning of micrometer-scale minerals with a high current density beam of Ga^+ produced by the metal/liquid gallium source. Synergy of FIB, TEM, and SEM provides an unprecedented opportunity to correlate observations on the host minerals, inclusions, dislocations, and any other characteristics over a wide range of scales: from tens of micrometers to atomic spacing of a few angstroms. Moreover, the FIB cutting "scar" remains on the polished surface of the sample, providing a permanent record of its location with respect to the microstructure of the rock and allowing repeated TEM examination of the precise area of interest if desired.

Electron-transparent foils from diamonds were prepared at GeoForschungsZentrum by using a single-beam FIB 200 (FEI) with an accelerating voltage of 30 kV. Technical details of this method are described in detail in refs. 16 and 22. Diamond foils were studied at an accelerating voltage of 200 kV with the scanning transmission electron microscope Technai 20 D435 X-Twin (FEI) equipped with a field emission gun and high-angle annular dark field (HAADF) detector. The high brightness source provided by the field emission gun has the ability to form an electron probe as small as 3 Å in diameter with low thermal energy spread. The selective collection efficiency of the HAADF detector provides an unprecedented opportunity for high spatial resolution and compositional imaging in STEM. The scanning transmission electron microscope is equipped with the electron dispersive x-ray spectrometer of the EDAX analytical system.

NanoSIMS. The nanoSIMS measurements were made on 1- to 5-μm diamonds included in garnets to study the ratio of stable isotopes of C^{12} and C^{13} (δC^{13}). NanoSIMS is a new generation of ion probe with a high spatial resolution Cs^+ beam as small as 50 nm in diameter (39). The nanoSIMS is capable of extending analysis to extremely small areas or volumes (50 nm) while retaining very high sensitivity (28, 40, 41). This derives from a revolutionary coaxial optical design of the ion gun and a new concept of the mass analyzer. The latter is due to a combination of a high intensity at high mass resolution and parallel secondary ion detection with six electron multipliers and one Faraday cup, which makes this instrument suitable for stable isotope measurements in submicrometer-size samples. It allows ppm to parts per billion trace level detection of all elements of the periodic table, including isotopic information. After comprehensive SEM image analysis, we used the CAMECA NanoSIMS-50 at the University of Tokyo for δC^{13} measurements on diamonds *in situ* in polished slides prepared from the quartzofeldspathic gneiss specimen from the Erzgebirge massif. The sample was coated with a thin film of gold in a vacuum chamber. The diamond standing out above the flat surfaces of the host garnets was easily identified with secondary electrons. Custom software was used to correct data for random outliers and possible stage drift that usually had a small effect on the final calculation of δC^{13}.

L.F.D. thanks Prof. Y. Sano for providing access to nanoSIMS at the University of Tokyo during her research as a fellow of the Japanese Society for the Promotion of Science and GeoForschungsZentrum for a travel grant. This work was supported by U.S. National Science Foundation Grants EAR 0229666 and EAR 0107118. IR measurements were performed at the U2A beamline at the National Synchrotron Light Source of Brookhaven National Laboratory, which is supported by the U.S. Department of Energy under Contract DE-AC02-98CH10886. The U2A beamline is also supported by COMPRES, the Consortium for Materials Properties Research in Earth Sciences, under U.S. National Science Foundation Cooperative Agreement Grant EAR 01-35554 and Carnegie/Department of Energy Alliance Center Contract DE-FC03-03N00144.

1. Ekimov EA, Sidorov VA, Bauer ED, Mel'nik NN, Curro NJ, Thompson JD, Stishov SM (2004) *Nature* 428:542–545.
2. Yokoya T, Nakamura T, Matsushita T, Muro T, Takano Y, Nagao M, Takenouchi T, Kawarada H, Oguchi T (2005) *Nature* 438:647–650.
3. Sobolev NV, Shatsky VS (1990) *Nature* 343:742–746.
4. Xu ST, Okay AI, Ji SY, Sengor AMC, Wen S, Liu YC, Jiang LL (1992) *Science* 256:80–82.
5. Yang J, Xu Z, Dobrzhinetskaya LF, Green HW, Pei X, Shi R, Wu C, Wooden JL, Zhang J, Wan Y, Li H (2003) *Terra Nova* 15:370–379.
6. Dobrzhinetskaya LF, Eide E, Korneliussen A, Larsen R, Millege J, Posukhova TV, Smith DS, Sturt BA, Taylor WR, Tronnes R (1995) *Geology* 23:597–600.
7. van Roermund HLM, Carswell DA, Drury MR, Heijboer TC (2002) *Geology* 30:959–962.
8. Massonne H-J (1999) in *Proceedings of the 7th International Kimberlitic Conference*, eds Gurney JJ, Gurney JM, Pascoe MD, Richardson SH (Red Roof Design, Cape Town, South Africa), Vol 2, pp 533–539.
9. Mposkos ED, Kostopoulos DK (2001) *Earth Planet Sci Lett* 192:497–506.
10. Dobrzhinetskaya LF, Green HW, Mitchell TE, Dickerson RM (2001) *Geology* 29:263–266.
11. Ogasawara Y (2005) *Elements* 1:91–96.
12. Cartigny P, de Corte K, Shatsky VS, Ader M, de Paepe P, Sobolev NV, Javoy M (2001) *Chem Geol* 176:265–281.
13. Stöckhert B, Gerya T (2005) *Terra Nova* 17:102–110.
14. Jones R, Briddon PR, Oberg S (1992) *Philos Mag Lett* 66:67–74.
15. Massonne H-J (2003) *Earth Planet Sci Lett* 216:347–364.
16. Dobrzhinetskaya LF, Green HW, Weschler M, Darus M, Wang Y-C, Massonne H-J, Stöckhert B (2003) *Earth Planet Sci Lett* 210:399–410.
17. Stöckhert B, Duyster J, Trepmann C, Massonne H-J (2001) *Geology* 29:391–394.
18. Dobrzhinetskaya LF, Green HW, Mitchell TE, Dickerson RM, Bozhilov KN (2003) *J Metamorph Geol* 21:425–437.
19. Chernov AA (1974) *J Cryst Growth* 24:11–31.
20. Langenhorst F (2003) *Mitt Oesterr Mineral Ges* 148:401–412.
21. Heaney PJ, Vicenzi EP, Giannuzzi LA, Livi KJ (2001) *Am Mineral* 86:1094–1099.
22. Wirth R (2003) *Eur J Mineral* 16:863–867.
23. Hwang SL, Chu HT, Yui TF, Shen P, Shertl HP, Liou JG, Sobolev NV (2006) *Earth Planet Sci Lett* 243:94–106.
24. Dobrzhinetskaya LF, Liu Z, Cartigny P, Zhang J, Tchkhetia NN, Green HW, II, Hemley RJ (2006) *Earth Planet Sci Lett* 248:325–334.
25. Hwang SL, Shen P, Chu HT, Yui TF (2000) *Science* 288:321–324.
26. Dobrzhinetskaya LF, Wirth R, Green HW (2005) *Terra Nova* 17:472–477.
27. Dobrzhinetskaya LF, Wirth R, Green HW (2005) *Earth Planet Sci Lett* 243:85–93.
28. Hoppe P (2006) *Appl Surf Sci* 252:7102–7106.
29. Massonne H-J, O'Brien PJ (2003) *Eur Mineral Union Notes Mineral* 5:145–187.
30. Chrenko RM, Tuft RE, Strong HM (1977) *Nature* 270:141–144.
31. Taylor WR, Canil D, Milledge HJ (1996) *Geochim Cosmochim Acta* 60:4725–4733.
32. Akaishi M, Yamaoka S (2000) *J Cryst Growth* 209:999–1003.
33. Hong SM, Akaishi M, Yamaoka S (1999) *J Cryst Growth* 200:326–328.
34. Dobrzhinetskaya LF, Renfro AP, Green HW (2004) *Geology* 10:869–872.
35. Pal'yanov YN, Sokol AG, Borzdov YM, Khokhryakov AF, Sobolev NV (1999) *Nature* 400:417–418.
36. Carr GL, Hanfland M, Williams GP (1995) *Rev Sci Instrum* 66:1643–1648.
37. Ochnishi T, Kawanami Y, Ishitani T (1990) *Jpn J Appl Phys Lett* 29:L188–L190.
38. Orloff J (1993) *Rev Sci Instrum* 64:1105–1130.
39. Conty C (2001) *Microsc Microanal* 7:142–149.
40. Hellebrand E, Snow JE, Mostefaoui S, Hoppe P (2005) *Contrib Mineral Petrol* 150:486–504.
41. Hoppe P, Mostefaoui S, Stephan T (2005) *Geochim Cosmochim Acta* 69:A523.